http://dx.doi.org/10.1090/conm/218/03005

Contemporary Mathematics
Volume **218**, 1998
B 0-8218-0988-1-03005-3

Domain Decomposition Methods for Flow in Heterogeneous Porous Media

Magne S. Espedal, Karl J. Hersvik, and Brit G. Ersland

1. Introduction

A reservoir may consist of several different types of sediments, which in general have different porosity, ϕ, absolute permeability, $\mathbf{K}$, relative permeabilities, k_{ri}, and capillary pressure P_c. In this paper we will study two phase, immiscible flow, in models consisting of one or two different types of sediment. Each of the sediments may be heterogeneous. The phases are water (w) and oil (o), but the results may easily be extended to groundwater problems where the phases may be water and air or a non aqueous phase.

Such models represent a very complex and computational large problem and domain decomposition methods are a very important part of a solution procedure. It gives a good tool for local mesh refinement in regions with large gradients such as fluid fronts, interfaces between different sediments or at faults. If the models are heterogeneous, parameters in the models may be scale dependent, which means that mesh coarsening may be possible in regions with small gradients.

Let $S = S_w$ denote the water saturation. Then the incompressible displacement of oil by water in the porous media can be described by the following set of partial differential equations, given in dimensionless form:

$$\nabla \cdot \mathbf{u} = q_1(\mathbf{x}, t), \tag{1}$$

$$\mathbf{u} = -\mathbf{K}(\mathbf{x}) M(S, \mathbf{x}) \nabla p, \tag{2}$$

$$\phi(\mathbf{x}) \frac{\partial S}{\partial t} + \nabla \cdot (f(S)\mathbf{u}) - \varepsilon \nabla \cdot (D(S, \mathbf{x}) \nabla S) = q_2(\mathbf{x}, t)\,. \tag{3}$$

Here, $\mathbf{u}$ is the total Darcy velocity, which is the sum of the Darcy velocities of the oil and water phases:

$$\mathbf{u} = \mathbf{u}_o + \mathbf{u}_w$$

1991 *Mathematics Subject Classification.* Primary 76T05; Secondary 35M20, 65M55, 65M25.

Key words and phrases. Reservoir models, Upscaling, Hierarchical basis, Domain Decomposition, Operator splitting.

Support from The Norwegian Research Council under the program PROPETRO and from VISTA, a research cooperation between the Norwegian Academy of Science and Letters and Statoil, is gratefully acknowledged.

©1998 American Mathematical Society

License or copyright restrictions may apply to redistribution; see http://www.ams.org/publications/ebooks/terms

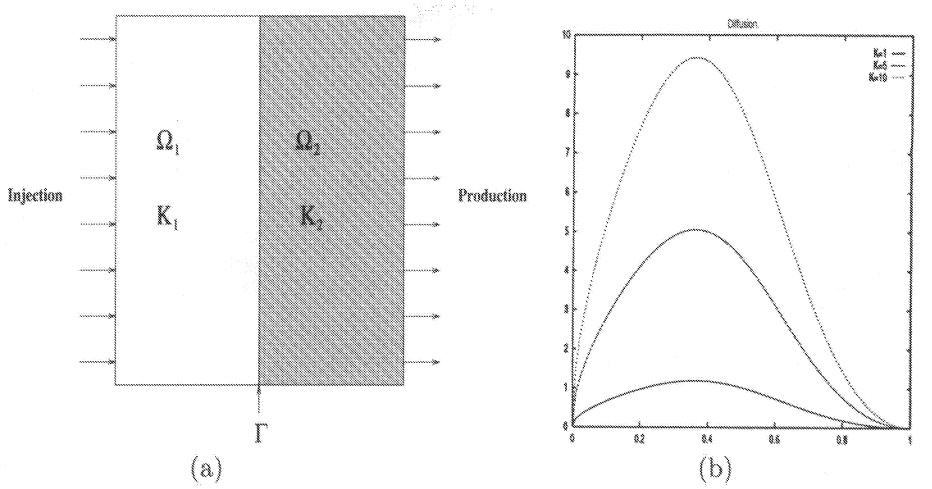

FIGURE 1. (a) Computational domain showing two different regions with different physical properties connected through an interior boundary Γ. (b) Capillary diffusion, as functions of saturation shown for permeabilities 1, 5 and 10.

Furthermore, p is the total fluid pressure given by $p = \frac{1}{2}(p_w + p_o)$, $q_i(\mathbf{x}, t), i = 1, 2$ denotes contribution from the injection and production wells in addition to capillary pressure terms, which are treated explicitly in (1). $\mathbf{K}(\mathbf{x})$ is the absolute permeability, $M(S, \mathbf{x})$ denotes the nonzero total mobility of the phases and $\phi(\mathbf{x})$ is the porosity. A reasonable choice for the porosity is $\phi = 0.2$. The parameter ε is a small $(10^{-1} - 10^{-4})$ dimensionless scaling factor for the diffusion.

Equation (3) is the fractional flow formulation of the mass balance equation for water. The fractional flow function $f(S)$ is typically a S shaped function of saturation., The capillary diffusion function $D(S, \mathbf{x})$ is a bell shaped function of saturation, S, and has an almost linearly dependence of the permeability $\mathbf{K}(\mathbf{x})$. Further, $D(0, \mathbf{x}) = D(1, \mathbf{x}) = 0$. In Figure 1, a capillary diffusion function is shown for different permeabilities.

For a complete survey and justification of the model we refer to [**5**]. We have neglected gravity forces, but the methods described can also be applied for models where gravity effects are included [**17**]. The following analytical form for the capillary pressure is chosen[**35**]:

$$P_C(S, \mathbf{x}) = 0.9\phi^{-0.9}\mathbf{K}^{-0.1}\frac{1 - S}{\sqrt{S}}, \tag{4}$$

We note that the capillary pressure depend on the permeability of the rock.

The phase pressures and the capillary pressure are continuous over a boundary Γ, separating two sediments. Furthermore, the flux must be continuous [**12, 14, 4, 23**] which gives the following internal boundary conditions:

$$P_C^{\Gamma-}(S^{\Gamma-}) = P_C^{\Gamma+}(S^{\Gamma+}) \tag{5}$$

$$(\mathbf{u}^{\Gamma-} - \mathbf{u}^{\Gamma+}) \cdot \mathbf{n}^{\Gamma} = 0 \tag{6}$$

License or copyright restrictions may apply to redistribution; see http://www.ams.org/publications/ebooks/terms

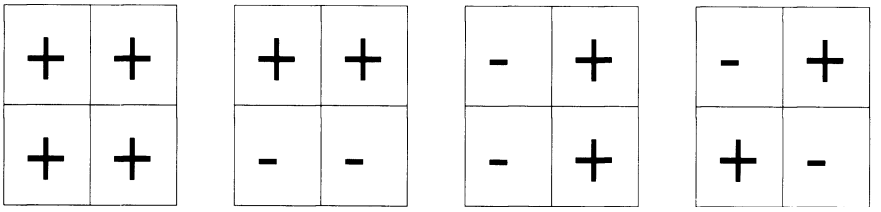

FIGURE 2. From left to right Γ_0, Γ_α, Γ_β, Γ_γ. The + and − sign represent the functional value +1 and -1. Γ_0 is the scaling function.

(7)
$$(f(S^{\Gamma-})\mathbf{u} - \varepsilon D^{\Gamma-}(S^{\Gamma-},\mathbf{x})\nabla S^{\Gamma-}) \cdot \mathbf{n}^\Gamma = (f(S^{\Gamma+})\mathbf{u} - \varepsilon D^{\Gamma+}(S^{\Gamma+},\mathbf{x})\nabla S^{\Gamma+}) \cdot \mathbf{n}^\Gamma.$$

Here $(\cdot)^{\Gamma-}$ and $(\cdot)^{\Gamma+}$ denote the left and right hand side value at the interior boundary Γ, and $\mathbf{n}^\Gamma$ is normal to the boundary.

Since the capillary pressure depends on both the saturation and the permeability, the continuity of the capillary pressure leads to discontinues saturation over the interior boundary. Also, the flux conservation (7) create large gradients in the saturation over an interior boundary separating two different sediments. This adds extra complexity to our problem especially when a saturation front passes an interface.

2. Representation of the Permeability

The permeability $\mathbf{K}$ may have several orders of variation and the geometrical distribution can be very different in the sediments. Further, fractures and faults add to the complexity. Therefore, we need a good method for the representation of $\mathbf{K}$. Hierarchical basis may be such a tool [**27, 18**].

The simplicity of the Haar system makes it an attractive choice for such a representation. Further it gives a permeability representation which is consistent with a domain decomposition solution procedure. We will restrict ourselves to two space dimensions and consider the unit square as our computational domain Ω. The Haar basis of scale 0 and 1, for two space dimension, is given by the set of functions in Figure 2.

On each mesh of 2×2 cells, any cell wise constant function can be given a representation as linear combinations of Γ_0, Γ_α, Γ_β and Γ_γ, where the coefficient of Γ_0 has a nonzero coefficient only for mesh of scale 0, which is the whole computational domain Ω. A 2-scale Haar multi resolution analysis, built on the scaling function Γ_0 [**6, 9**], will be used to represent the permeability.

Let the absolute permeability $\mathbf{K}$ be a cell-wise constant function on Ω with 2^{N+1} cells in each direction.

Then $\mathbf{K}$ can then be expanded in terms of the Haar basis:

$$\mathbf{K} = \mathbf{K}_0\Gamma_0 + \sum_{i=1}^{N}\sum_{j=0}^{2^N}\sum_{k=0}^{2^N}\sum_{l=\alpha,\beta,\gamma} \mathbf{K}_{ijkl}\Gamma_{ijkl} \tag{8}$$

where the index i gives the scale and j and k give the translations of the two dimensional wavelet Γ_{ijkl}.

License or copyright restrictions may apply to redistribution; see http://www.ams.org/publications/ebooks/terms

We should note that this representation is easily extended to three space dimensions. If the permeability is given by a tensor, the wavelet representation should be used for each of the components. Also, other types of wavelet may be used. Especially if an overlapping domain decomposition method is used, a less localised wavelet representation should be useful.

3. Solution procedure

The governing equations (1), (2) and (3) are coupled. A sequential, time marching strategy is used to decouple the equations. This strategy reflects the different natures of the elliptic pressure equation given by (1) and (2), and the convection dominated parabolic saturation equation (3). The general solution strategy is published earlier [**15, 10, 25, 8, 21**], so we only give the main steps in the procedure.

3.1. Sequential Solution Procedure:

- **Step 1:**
  For $t \in [t_n, t_{n+1}]$, solve the pressure and velocity equations (1, 2). The velocity is a smoother function in space and time than the saturation. Therefore we linearize the pressure and velocity equations by using the saturation from the previous time step, $S = S(t_n)$. The pressure equation is solved in a weak form, using a standard Galerkin method with bilinear elements [**2, 31**].

  Then the velocity is derived from the Darcy equation (2), using local flux conservation over the elements [**31**]. This gives the same accuracy for the velocity field as for the pressure. The mixed finite element method would be an alternative solution procedure. In many cases, it is not necessary to solve the pressure for each timestep.
- **Step 2:**
  A good handling of the convective part of the saturation equations, is essential for a fast and accurate solution for S. We will use an operator splitting technique where an approximate saturation $\tilde{S}$ is calculated from a hyperbolic equation:
  For $t \in [t_n, t_{n+1}]$, with $\mathbf{u}$ given from Step 1, solve:

$$\frac{d\tilde{S}}{d\tau} \equiv \phi \frac{\partial \tilde{S}}{\partial t} + \nabla \cdot (\bar{f}(\tilde{S})\mathbf{u}) = 0 \tag{9}$$

  where $\bar{f}$ is a modified fractional flow function [**15, 8, 21**].
- **Step 3:**
  The solution $\tilde{S}$ provide a good approximation of the time derivative and the nonlinear coefficients in (3).
  For $t \in [t_n, t_{n+1}]$, and $S_0 = \tilde{S}$, solve:

$$\frac{\partial S_i}{\partial \tau} + \nabla \cdot (b(S_{i-1})S_i\mathbf{u} - \mathbf{D}(S_{i-1}) \cdot \nabla S_i) = q_2(\mathbf{x}, t) \tag{10}$$

  for $i = 1, 2, 3....$ until convergence, where $b(S)S = f(S) - \bar{f}(S)$. Equation (10) is solved in a weak form [**15, 8**], using optimal test functions [**3**].

License or copyright restrictions may apply to redistribution; see http://www.ams.org/publications/ebooks/terms

- **Step 4:**
  Depending on the strength of the coupling between the velocity and the saturation equation, the procedure may be iterated.

3.2. Domain decomposition. The pressure (1), (2) and saturation equation (10) represent large elliptic problems. The equations are solved by using a preconditioned iterative procedure, based on domain decomposition [**32**]. The procedure allows for adaptive local grid refinement, which gives a better resolution at wells and in regions with large permeability variations such as interfaces between two types of sediments. The procedure also allows for adaptive local refinement at moving saturation fronts. Assuming a coarse mesh Ω_C on the computational domain Ω, we get the following algorithm [**29, 8, 34, 33**]:

1. Solve the splitted hyperbolic saturation equation (9) on the coarse grid Ω_C, by integrating backwards along the characteristics.
2. Identify coarse element that contain large gradients in saturation and activate refined overlapping/non overlapping sub grids Ω_k to each of these.
3. Solve equation (9) on the refined sub grids Ω_k, by integrating backwards along the characteristics.
4. Using domain decomposition methods, solve the complete saturation equation with the refined coarse elements. The characteristic solution $\tilde{S}$ is used as the first iteration of the boundary conditions for the sub domains Ω_k .

As is well known, algorithms based on domain decompositions have good parallel properties [**32**].

We will present result for 2D models, but the procedure has been implemented and tested for 3D models [**16**].

4. Coarse Mesh Models

With the solution procedure described in Section 3, pressure, velocity and saturation will be given on a coarse mesh in some regions a and on a refined mesh in the remaining part of Ω. This means that the model equations have to be given for different scales. Several upscaling techniques are given in the literature [**22, 1, 11, 26, 18, 7, 30, 24**]. In this paper, we will limit the analysis to the upscaling of the pressure equation. The upscaling of the saturation equation is less studied in the literature [**1, 24**].

The goal of all upscaling techniques is to move information from a fine grid to a coarser grid without loosing significant information along the way. A quantitative criteria is the conservation of dissipation:

$$e = \mathbf{K}\nabla p \cdot \nabla p \tag{11}$$

A related and intuitively more correct criteria, is the conservation of the mean fluid velocity $\langle \mathbf{v} \rangle$, given by:

$$\begin{aligned} \langle \mathbf{v} \rangle &= -\mathbf{K}_{eff} \nabla \langle p \rangle \\ \nabla \cdot \langle \mathbf{v} \rangle &= 0 \end{aligned} \tag{12}$$

where $\mathbf{K}_{eff}$ is an effective permeability.

In our approach it is natural to use conservation of the mean velocity as the upscaling criteria, although the method also conserves dissipation fairly well [**18**].

License or copyright restrictions may apply to redistribution; see http://www.ams.org/publications/ebooks/terms

4.1. Wavelet upscaling. A Multi Resolution Analysis (MRA), [**9**], defined on $L^2(R) \times L^2(R)$ consists of a nested sequence of closed subspaces of $L^2, \times L^2$ such that:

$$\cdots \subset V_1 \subset V_0 \subset V_{-1} \subset \cdots \tag{13}$$

$$\bigcup_{j \in Z} V_j = L^2(R) \times L^2(R) \tag{14}$$

$$\bigcap_{j \in Z} V_j = \{0\} \tag{15}$$

$$V_{j+1} = V_j \cup W_j \tag{16}$$

$$f(x) \in V_j \iff f(2x) \in V_{j+1} \tag{17}$$

Here, W_j is the orthogonal complement of V_j in V_{j+1}. The permeability given by (8) satisfies such a hierarchical representation. Let $j = 0$ and $j = J$ be respectively the coarsest and finest scale to appear in $\mathbf{K}$. Upscaling in this context is to move information form scale $j = J$ to a coarser scale $j = M$, $M \leq J$.

In signal analysis, "highcut" filters are commonly used to clean a signal from its high frequency part which is considered to be negligible noise. We will apply to same reasoning on $\mathbf{K}$. Such an upscaling will keep all large scale information, while variation on scales below our course grid will be neglected in regions where the flow has a slow variation. Moderate fine scale changes in the permeability, give rise to heterogeneous fingers [**24**] and have little influence on the global transport. But this upscaling technique is only valid in the case that the coefficients on the scales $J, J-1, \ldots, M$ are small compared to the coefficients on a lower scale. This would not be the case for narrow high permeability zones. However, in regions with high permeability channels, the solutions will contain large gradients, which mean that we should use a refined grid to resolve the dynamics. A coarse grid solution based on upscaling, will loose too much information in such regions.

4.2. Highcut upscaling. We will give an example of the highcut upscaling techniques on an anisotropic permeability field. Such a field is chosen because it is difficult to handle using simple mean value techniques. The coefficients which determine the permeability field at each scale are read from a file, but if we want to work with measured permeability fields, a subroutine can determine the coefficients on each scale recursively using standard two scale relations from the wavelet theory, [**9**].

The permeability field is generated by introducing large coefficients on a relatively low level. The goal is to model a case where we may have several regimes of permeability which on their own may be isotropic, but when put together constitute a very complex reservoir.

Figure 3 shows the permeability field for a highcut upscaling as 3-D histograms. We can clearly see the complexity and anisotropy of the permeability field. Upscaling to scale 3 gives a massive loss of information, because the scale 4 coefficient are fairly large.

Table 1 displays the coefficients used. The aspect ratio between the highest and lowest permeability is about 10 in this case [**18**]. The highest scale is 7 which gives $2^7 \times 2^7$ cells, and the permeability value on scale 0 is 1.0. K_α, K_β and K_γ are the coefficients of Γ_α, Γ_β and Γ_γ respectively (2).

License or copyright restrictions may apply to redistribution; see http://www.ams.org/publications/ebooks/terms

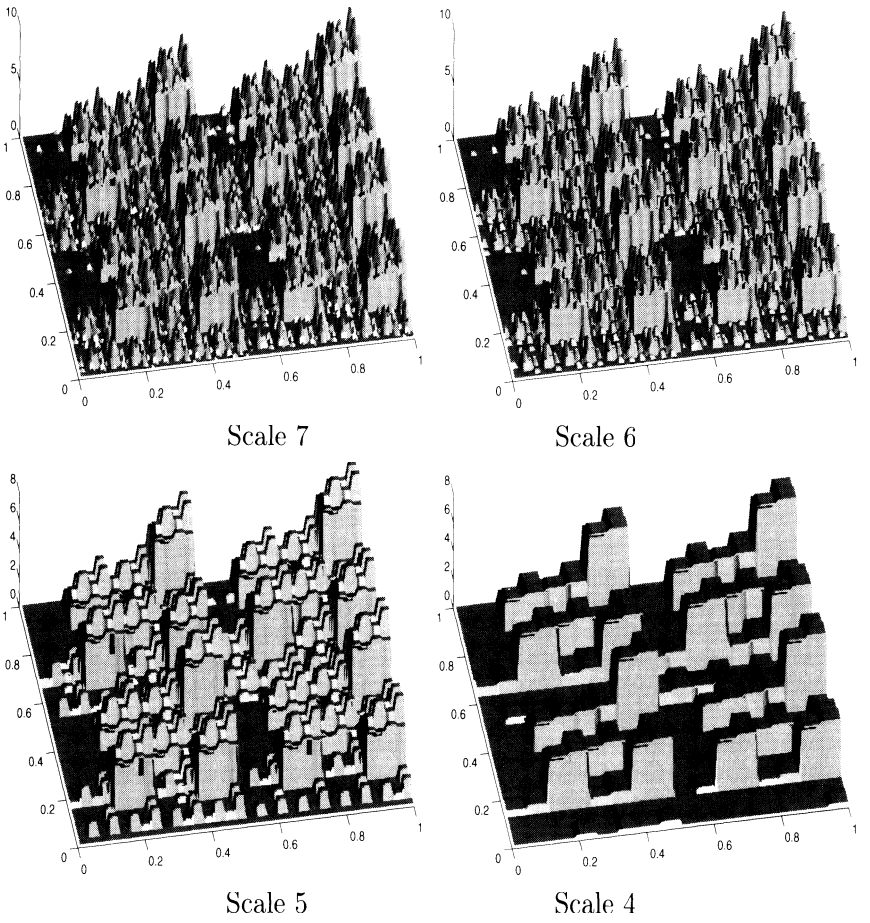

FIGURE 3. The figure shows the permeability field for a highcut upscaling in a 3-D histograms. Scale 7 $\rightarrow$ 128×128 cells, scale 6 $\rightarrow$ 64×64 cells, scale 5 $\rightarrow$ 32×32 cells and scale 4 $\rightarrow$ 16×16 cells.

TABLE 1. The table show the value of the coefficients on each level.

Level	K_α	K_β	K_γ
1	0.3	0.1	0.2
2	0.0	1.0	0.9
3	1.0	0.9	0.8
4	-0.4	0.3	0.2
5	0.5	0.2	0.3
6	0.1	-0.2	-0.3
7	0.2	0.1	0.0

5. Model error

As clearly shown in Figure 3, upscaling of permeability introduces modeling error. In order to develop a domain decomposition based simulator, the model has to be given on different scales. Therefore, we need an a posteriori error estimate of the modeling error introduced by the upscaling if we want to control the total

License or copyright restrictions may apply to redistribution; see http://www.ams.org/publications/ebooks/terms

error in the computation. Such an error estimate can give the base for an adaptive local refinement procedure for the simulation of heterogeneous porous media.

Defining the bilinear form:

$$A : H^1(\Omega) \times H_0^1(\Omega) \mapsto R$$

$$A(p, \phi) = \int_\Omega \nabla p \cdot \mathbf{K} \nabla \phi d\mathbf{x} \tag{18}$$

Then, the fine scale weak form of the pressure equation (1, 2) is given by:

Find $p \in H^1(\Omega)$, such that

$$A(p, \phi) = (q_1, \phi), \qquad \forall \phi \in H_0^1(\Omega) \tag{19}$$

Denoting the upscaled permeability tensor by $\mathbf{K}^0$, we get the equivalent upscaled model:

Find $p^0 \in H^1(\Omega)$, such that

$$A^0(p^0, \phi) = (q, \phi), \qquad \forall \phi \in H_0^1(\Omega) \tag{20}$$

The modeling error introduced by replacing the fine scale permeability tensor with an upscaled permeability tensor may be given by:

$$e_{model} = \|\mathbf{v} - \mathbf{v^0}\| \tag{21}$$

where $\|\cdot\|$ is a norm defined on $L^2(\Omega) \times L^2(\Omega)$. If we define a norm as given in [**26**], we can avoid the appearence of the fine scale solution on the right hand side in the error estimate :

Let $\mathbf{w} \in L^2(\Omega) \times L^2(\Omega)$, then the fine scale-norm $\|\cdot\|_{\mathbf{K}^{-1}}$ is given by:

$$\|\mathbf{w}\|^2_{\mathbf{K}^{-1}} = \int_\Omega (\mathbf{w}, \mathbf{K}^{-1}\mathbf{w}) dx \tag{22}$$

Where $(\cdot, \cdot)$ is the Euclidean inner product on R^2. This is an L^2 norm with the weight function $\mathbf{K}^{-1}$. If we choose $\mathbf{K}$ as the weight function we get the energy norm, which is consistent with (22):

$$\|w\|^2_{\mathbf{K}} = A(w, w) = \int_\Omega \nabla w \cdot \mathbf{K} \nabla w dx \tag{23}$$

These norms will also appear in a mixed finite element formulation.

The following can be proved [**18, 26**]:

5.1. A posteriori error estimate. Let $\mathbf{K}$ and $\mathbf{K^0}$ be symmetrical and positive definite tensors. Assume that $\mathbf{K^0}$ is the result of an upscaling technique applied to $\mathbf{K}$, such that:

$$\int_\Omega [\mathbf{K}^0 \nabla p^0(\mathbf{K}^0), \nabla p^0(\mathbf{K}^0)] dx \leq \int_\Omega [\mathbf{K} \nabla p, \nabla p] dx \tag{24}$$

and

$$\|\mathbf{K}\|_{L^\infty} \leq M \text{ and } \|\mathbf{K}^0\|_{L^\infty} \leq m \leq M \tag{25}$$

Let p^0 and p be solutions of respectively eq.(20) and eq. (19), and let $\mathbf{v}$ and $\mathbf{v}^0$ be the velocities given by $\mathbf{v} = -\mathbf{K}\nabla p$ and $\mathbf{v}^0 = -\mathbf{K}^0 \nabla p^0$. We have the following error estimate:

License or copyright restrictions may apply to redistribution; see http://www.ams.org/publications/ebooks/terms

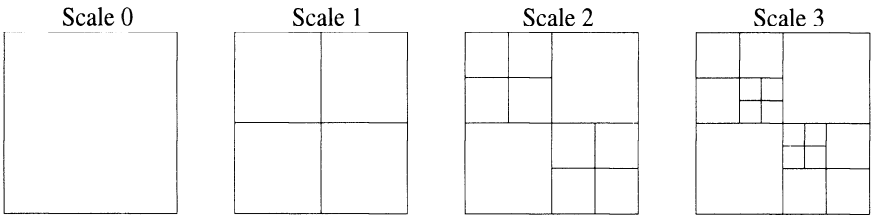

FIGURE 4. The figure shows a nested sequence of subdomains, $\Omega_i \subset \Omega$.

$$\|\mathbf{v} - \mathbf{v}^0\|_{\mathbf{K}^{-1}} \leq \|\mathbf{I}_0 \mathbf{v}^0\|_{\mathbf{K}^{-1}} \tag{26}$$

and

$$\|p - p^0\|_{\mathbf{K}} \leq \|\mathbf{I}_0 \nabla p^0\|_{\mathbf{K}} \tag{27}$$

where $(\mathbf{I}_0)^2 = \mathbf{I} - \mathbf{K}^{-1}\mathbf{K}^0$

The assumption (24) states that the dissipation in the problem is constant or decreasing during upscaling. Conservation of dissipation is one of the criteria used for judging the quality of an upscaling procedure see Section 4. The permeability representation given in Section 2 is consistent with the assumptions given in the theorem.

The aposteriori estimate of the modeling error is built on the results in [**26**]. It is proved [**26**] that the upscaling based on this norm gives very good results and as noted, the estimate does not involve the fine scale solution. The error estimate gives the basis for an adaptive upscaling technique. Together with domain decomposition, it gives a strong modeling procedure. The following algorithm is consistent with the hierarchical permeability representation given in Section 2:

Algorithm for an Adaptive Domain Decomposition Solution
Solve on scale 0. (Global coarse grid solve) This gives P^0_Ω and $\mathbf{v}^0_\Omega$
While(*error* $\geq$ *tol and scale* $\leq$ *maxscale*)
  Solve on all active local domains using the MRA representation.
  (After this step our data structure contains only inactive domains.)
  for($i = 1$; $i \leq$ *number_of_domains_on_this_scale;* $i++$)
    if(*local_error* $\geq$ *tol*)
      Generate four new active subdomains of this local domain.
    end if
    if(*local_error* $\geq$ *local_error_prev*)
      local_error_prev = local_error
    end if
  end for
  error = local_error_prev
end while(...)

The separation of the domains into two classes, active and non-active, ensures that we do not waste time recomputing on domains which are not split up as we move up in the hierarchy. Thus the iteration will just involve these four sub domains

License or copyright restrictions may apply to redistribution; see http://www.ams.org/publications/ebooks/terms

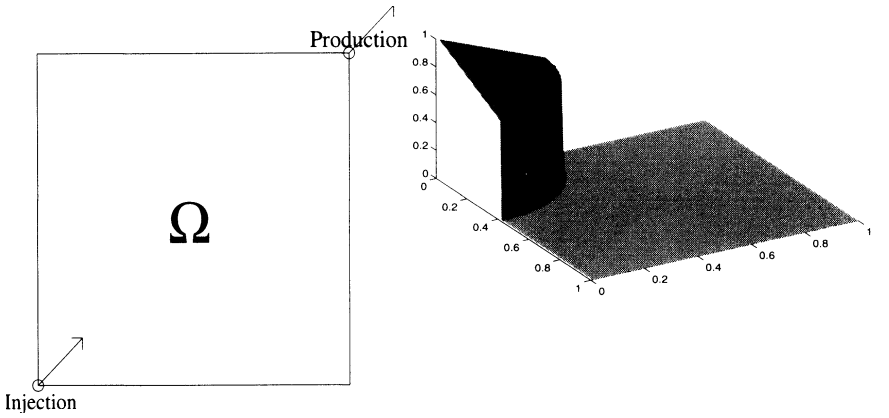

(a) (b)

FIGURE 5. Experimental setting (a) and initial saturation profile (b).

if only one domain is refined. On the other hand if two neighboring domains are refined, the iteration process will involve eight domains. Figure 4 shows a situation where all scales from scale 1 to scale 3 are present in the solution.

6. Numerical experiments

In this section we will present numerical experiments to demonstrate the effect of the error estimate and the "high-cut" upscaling technique. The computations will be based on the permeability data given by Figure 3. All experiments are based on the "quarter of a fivespot" problem. Our computational domain will be the unit square. Figure 5 shows a typical configuration along with the initial saturation profile.

6.1. Reference Solution. The main objective of the experiment is to better understand the behavior of the error estimate in theorem (5.1) together with domain decomposition methods, based on local solvers [**18**]. We define the effectivity indices, $\eta_{\mathbf{K}}$, [**28**], measuring the quality of the error prediction as:

$$\eta_{\mathbf{K}} = \frac{\|\mathbf{I}^0\mathbf{v}^0\|^2_{\mathbf{K}^{-1}}}{\|\mathbf{v}^0 - \mathbf{v}\|^2_{\mathbf{K}^{-1}}} \tag{28}$$

To create a reference solution, we apply a global solver and identical grid on all scales. This grid has 128×128 cells and corresponds to scale 7. This means that on scale 7 each cell is assigned a permeability value and we use scale 7 as our reference scale. Figure 6 show the velocity and saturation fields for scale 7 and 4. The results are based on the permeability field given by Figure 3. The most apparent feature is the complexity in the fields. Both absolute value and direction changes radically over short distances. The saturation are shown at $t = 0.14$. We see that the main flowpattern are the same for the models, but as expected, some of the small scale variation is lost on scale 4 [**24**].

License or copyright restrictions may apply to redistribution; see http://www.ams.org/publications/ebooks/terms

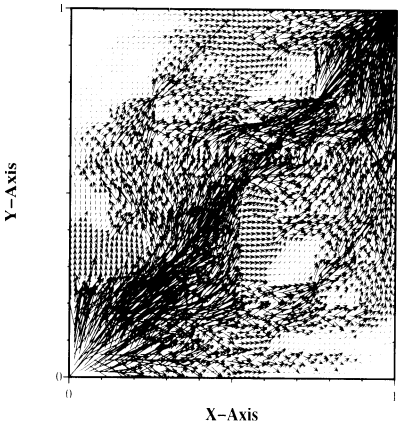

(a) Velocity field for Scale 7

(b) Velocity field for Scale 4

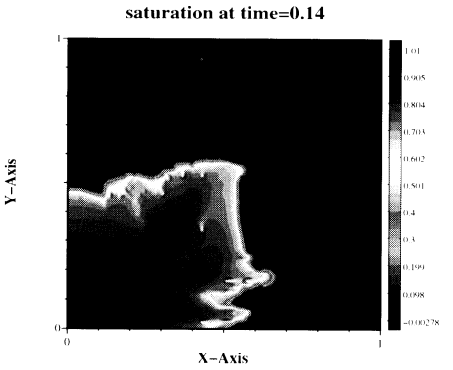

(c) Saturation field for Scale 7

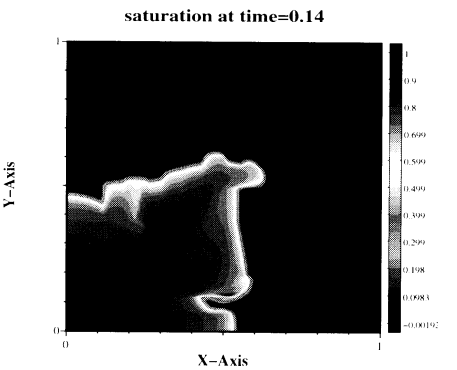

(d) Saturation field for Scale 4

FIGURE 6. The figure shows the velocity and saturation fields for a highcut upscaling with global solvers. Figure (a) and (c) represent the reference solution. Scale 7 $\rightarrow$ 128×128 cells and scale 4 $\rightarrow$ 16×16 cells.

License or copyright restrictions may apply to redistribution; see http://www.ams.org/publications/ebooks/terms

TABLE 2. The effectivity indices for $\eta_{\mathbf{K}}$ for scale 4 - 6

Scale	$\eta_{\mathbf{K}}$
6	1.45
5	1.48
4	1.54

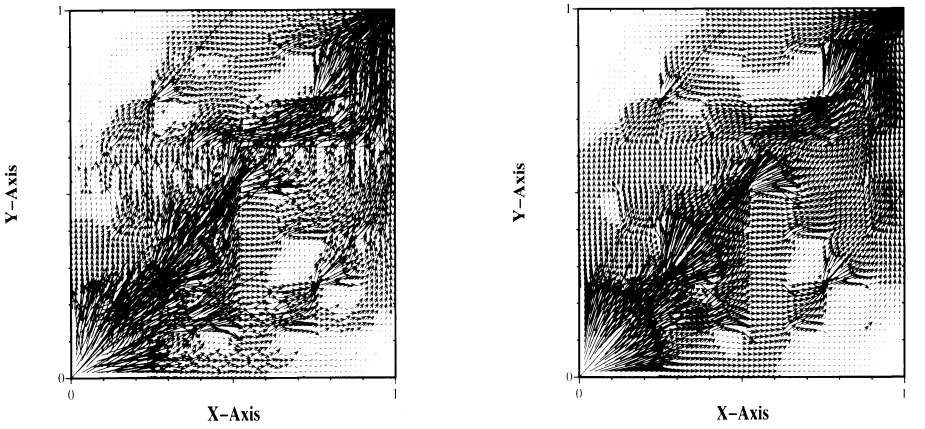

(a) $\eta_{\mathbf{K}} = 1.35$, 24×24 sub domains (b) $\eta_{\mathbf{K}} = 1.75$, 9×9 sub domains

FIGURE 7. The figure shows the velocity field for a highcut upscaling technique coupled with localized solvers through the adaptive upscaling algorithm. The results should be compared with the reference solution (Scale 7) given in Figure 6

Table 2 shows the effectivity indices for each scale, which shows that $\eta_{\mathbf{K}}$ vary as expected.

It can be shown that dissipation is fairly well conserved in this case [**18**].

6.2. Local solvers. In this section we will test the local adaptive upscaling algorithm (5.1) together with local solvers [**18**]. To capture the global communication in the problem we had to apply coarse grid solvers at each scale. This was apparent only when the velocity field showed radical changes in both absolute value and direction. For permeability fields where these changes were less rapid a coarse grid solver was no longer necessary [**18**]. The domain decomposition has been based on the multiplicative Schwarz algorithm. Figure 7 shows the velocity field for an upscaling with the adaptive algorithm (5.1). The plot shows the velocity field corresponding for two values of the error estimate. Note that even when the

License or copyright restrictions may apply to redistribution; see http://www.ams.org/publications/ebooks/terms

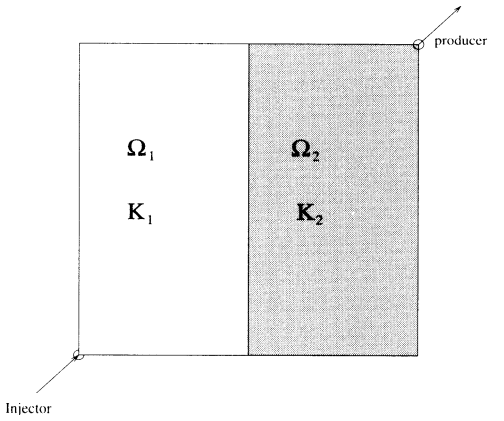

FIGURE 8. The computational domain Ω.

quality of the error estimation is poor, $\eta_{\mathbf{K}} = 1.75$, most of the global transport is still captured using only 9×9 local domains. The results in Figure 7 should be compared to the reference velocity field given in Figure 6. As the quality of the error estimation improves the solution is almost identical to the reference solutions [**18**] and even for $\eta_{\mathbf{K}} = 1.35$, 24×24 sub domains, the velocity field is very accurate. The iteration error was chosen very small such that the iteration error did not influence on the estimate of the modeling error. The two solutions will, however, never be identical due to large areas where the mean velocities are small such that the mesh is not refined. The differences are not visible on the plots and have only a negligible effect on the global flow.

In most cases, the local coarsening of meshes by upscaling, will reduce the computational cost substantially. With the adapive technique proposed, the modeling error can still be kept under control.

7. Two sediment model

The solution procedure described in Section 3 can be extended to models consisting of several types of sediments. We will limit the presentation to a two sediment model.

We consider a rectangular domain Ω which has an interior boundary Γ, at $x = 0.5$, separating the two sediments. We assume that both Ω_1 and Ω_2 are homogeneous. All the parameters like absolute and relative permeability and capillary pressure, may be discontinues across such interfaces [**36, 19, 12, 13, 14, 20**]. We will assume that only the absolute permeability is discontinues across Γ, which means that also the capillary pressure (4) is discontinues. In order to satisfy the interface relations (5) and (7), the saturation S also has to be discontinues across Γ.

This discontinuity is handled by introducing discontineous trial functions [**12, 14**] in the weak formulation of the saturation equation (10). The jump discontinuity in the trialfunctions [**12, 14**] are determined from the interface relations (5) and (7). A problem with an injector well in lower left corner and a production well in upper right corner, as shown in Figure 8 is studied. The numerical results obtained with the adaptive local grid refinement at the front and a fixed local refinement at the interior boundary in [**12, 34, 13**] are compared

License or copyright restrictions may apply to redistribution; see http://www.ams.org/publications/ebooks/terms

TABLE 3. Time and well data for the test cases.

Parameter	value	Decription
dt	0.001	time step
t	[0,48]	time intervall
inj_ rate	0.2	injection rate
prod_ rate	-0.2	production rate

TABLE 4. The permeability fields defining test cases a and b.

case:	$K(\Omega_1)$	$K(\Omega_2)$
a	1.0	0.1
b	0.1	1.0

with equivalent results computed on a uniform global mesh. The local refinement is obtained by domain decomposition methods described in Section 3. The agreement between the two approaches is very good.

We choose the same type of initial condition for the saturation as given in Figure 5. This represents an established front, located away from the injection well.

Saturation solutions will be shown at four time levels, $t = 0.24$, and $t = 0.48$. Input data are given in Table 3 and Table 4, while the injection and production rates are given in Table 3 together with the time parameters.

Figure 9 gives computed saturations for the test cases a and b in Table 4. In Figure 9 (a) and (c) (Testcase a) water is injected in a high permeability sediment and oil is produced in a low permeable sediment. In Figure 9 (b) and (d) (Testcase b) water is injected in a low permeable sediment, and oil is produced in a high permeable sediment.

The total Darcy velocity and the capillary diffusion depend on the permeability field $\mathbf{K}$. The effects of different permeabilities and capillary forces in the two regions Ω_1 and Ω_2 combined with the effect of the boundary conditions (5), (7), are clearly seen in Figure 9 (a) - (d) . The saturation jump at the internal boundary is positive for testcase a and negative for testcase b [**12, 14**].

We observe that the saturation front is more smeared in the high permeable region than in the low permeable region, consistent with the magnitude of the diffusion term as given in Figure 1.

As noted, the results shown are computed both with uniform grids and with local refinement based on domain decomposition [**12**]. The grid is adaptively refined at the saturation fronts [**8, 12**] and at the internal boundary Γ. Except for small interpolation effects at the boundary between the coarse and the refined meshes, the results are similar.

The results are extended to models where both absolute and relative permeability and capillary pressure are given by different functional form in the two sediments [**12, 14**]. Work is under way to extend the models to heterogeneous multisediment models and models with fractures. The local refinement of meshes at interfaces and saturation fronts or the local coarsening of meshes by upscaling, will reduce the computational cost substantially.

License or copyright restrictions may apply to redistribution; see http://www.ams.org/publications/ebooks/terms

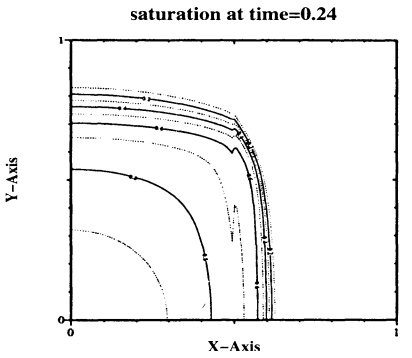

(a) $t = 0.24$

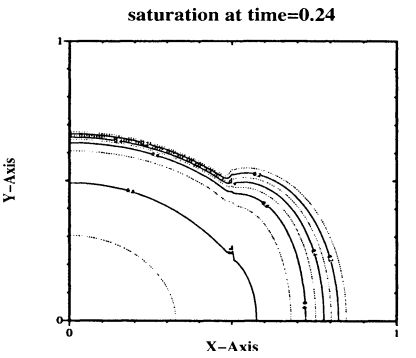

(b) $t = 0.24$

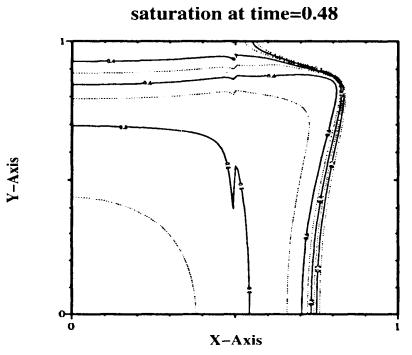

(c) $t = 0.48$

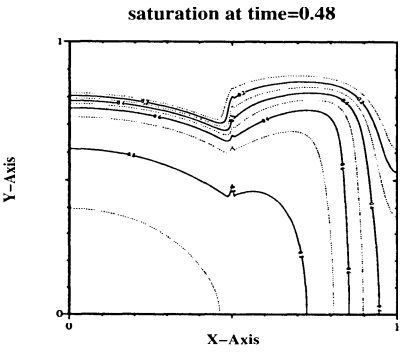

(d) $t = 0.48$

FIGURE 9. Saturation profile for five spot problem at time levels $t = 0.24$, and $t = 0.48$. $K(\Omega_1) = 1$ and $K(\Omega_2) = 0.1$ in Figure (a) and (c). $K(\Omega_1) = 0.1$ and $K(\Omega_2) = 1$ in Figure (b) and (d).

8. Conclusion

In this work we have focused on solution techniques for two phase porous media flow, where the models may be heterogeneous or consist of different types of sediments. An adaptive upscaling technique is given. This gives a flexible and powerful procedure for local grid refinement based on domain decomposition. Work is under way to extend the methods to more complex models like flow in fractured rock.

License or copyright restrictions may apply to redistribution; see http://www.ams.org/publications/ebooks/terms

References

1. B. Amazine, A Bourgeat, and J. V. Koebbe, *Numerical simulation and homogenization of diphasic flow in heterogeneous reservoirs*, Proceedings II European conf. on Math. in Oil Recovery (Arle, France) (O. Guillon D. Guerillot, ed.), 1990.
2. O. Axelsson and V.A. Barker, *Finite element solution of boundary value problems*, Academic Press, London, 1984.
3. J.W. Barrett and K.W. Morton, *Approximate symmetrization and Petrov-Galerkin methods for diffusion-convection problems*, Computer Methods in Applied Mechanics and Engineering **45** (1984), 97–122.
4. Ø. Bøe, *Finite-element methods for porous media flow*, Ph.D. thesis, Department of Applied Mathematics, University of Bergen, Norway, 1990.
5. G. Chavent and J.Jaffre, *Mathematical models and finite elements for reservoir simulation*, North-Holland, Amsterdam, 1987.
6. C. K. Chu, *An introduction to wavelets*, Academic Press, Boston, 1992.
7. G. Dagan, *Flow and transport in porous formations*, Springer-Verlag, Berlin-Heidelberg, 1989.
8. H.K. Dahle, M.S. Espedal, and O. Sævareid, *Characteristic, local grid refinement techniques for reservoir flow problems*, Int. Journal for Numerical Methods in Engineering **34** (1992), 1051–1069.
9. I. Daubechies, *Ten lectures on wavelets*, Conf. Ser.Appl. Math. SIAM, Philadelphia, 1992.
10. J. Douglas, Jr. and T.F. Russell, *Numerical methods for convection-dominated diffusion problems based on combining the method of characteristics with finite element or finite difference procedures*, SIAM Journal on Numerical Analysis **19** (1982), 871–885.
11. L. J. Durlofsky and E. Y. Chang, *Effective permeability of heterogeneous reservoir regions*, Proceedings II European conf. on Math. in Oil Recovery (Arle, France) (O. Guillon D. Guerillot, ed.), 1990.
12. B. G. Ersland, *On numerical methods for including the effect of capillary presure forces on two-phase, immmiscible flow in a layered porous media*, Ph.D. thesis, Department of Applied Mathematics, University of Bergen, Norway, 1996.
13. B. G. Ersland and M. S. Espedal, *Domain decomposition method for heterogeneous reservoir flow*, Proceedings Eight International Conference on Domain Decomposition Methods, Beijing, 1995 (London) (R. Glowinski, J. Periaux, Z-C. Shi, and O. Widlund, eds.), J.Wiley, 1997.
14. M. S. Espedal, B. G. Ersland, K. Hersvik, and R. Nybø, *Domain decomposition based methods for flow in a porous media with internal boundaries*, Submitted to: Computational Geoscience, 1997.
15. M. S. Espedal and R.E. Ewing, *Characteristic Petrov-Galerkin subdomain methods for two-phase immiscible flow*, Computer Methods in Applied Mechanics and Engineering **64** (1987), 113–135.
16. J. Frøyen and M. S. Espedal, *A 3D parallel reservoir simulator*, Proceedings V European conf. on Math. in Oil Recovery (Leoben,Austria) (M. Kriebernegg E. Heinemann, ed.), 1996.
17. R. Hansen and M. S. Espedal, *On the numerical solution of nonlinear flow models with gravity*, Int. J. for Num. Meth. in Eng. **38** (1995), 2017–2032.
18. K. Hersvik and M. S. Espedal, *An adaptive upscaling technique based on an a-priori error estimate*, Submitted to: Computational Geoscience, 1997.
19. J. Jaffre, *Flux calculation at the interface between two rock types for two-phase flow in porous media*, Transport in Porous Media **21** (1995), 195–207.
20. J. Jaffre and J. Roberts, *Flux calculation at the interface between two rock types for two-phase flow in porous media*, Proceedings Tenth International Conference on Domain Decomposition Methods, Boulder, (1997).
21. K. Hvistendahl Karlsen, K. Brusdal, H. K. Dahle, S. Evje, and K. A. Lie, *The corrected operator splitting approach applied to nonlinear advection-diffusion problem*, Computer Methods in Applied Mechanics and Engineering (1998), To appear.
22. P. R. King, *The use of renormalization for calculating effective permebility*, Transport in Porous Media **4** (1989), 37–58.
23. T. F. M. Kortekaas, *Water/oil displacement characteristics in crossbedded reservoir zones*, Society of Petroleum Engineers Journal (1985), 917–926.
24. P. Langlo and M. S. Espedal, *Macrodispersion for two-phase immiscible flow in porous media*, Advances in Water Resources **17** (1994), 297–316.

License or copyright restrictions may apply to redistribution; see http://www.ams.org/publications/ebooks/terms

25. K. W. Morton, *Numerical solution of convection-diffusion problems*, Applied Mathematics and Mathematical Computation, 12, Chapman & Hall, London, 1996.
26. B. F. Nielsen and A. Tveito, *An upscaling method for one-phase flow in heterogenous reservoirs; a weighted output least squares approach*, Preprint, Dep. of informatics, Univ. of Oslo, Norway, 1996.
27. S. Nilsen and M. S. Espedal, *Upscaling based on piecewise bilinear approximation of the permeability field*, Transport in Porous Media **23** (1996), 125–134.
28. J. T. Oden, T. Zohdi, and J. R. Cho, *Hierarchical modelling, a posteriori error estimate and adaptive methods in computational mechanics*, Proceedings Comp. Meth. in Applied Sciences (London) (J. A. Desideri et.al., ed.), J. Wiley, 1996, pp. 37–47.
29. R. Rannacher and G. H. Zhou., *Analysis of a domain splitting method for nonstationary convection-diffuion problems*, East-West J. Numer. math. **2** (1994), 151–174.
30. Y. Rubin, *Stochastic modeling of macrodispersion in heterogeneous poros media*, Water Resources Res. **26** (1991), 133–141.
31. O. Sævareid, *On local grid refinement techniques for reservoir flow problems*, Ph.D. thesis, Department of Applied Mathematics, University of Bergen, Norway, 1990.
32. B. Smith, P. Bjørstad, and W. Gropp, *Domain decomposition*, Cambridge University Press, Camebridge, 1996.
33. X. C. Tai and M. S. Espedal, *Space decomposition methods and application to linear and nonlinear elliptic problems*, Int. J. for Num. Meth. in Eng. (1998), To appear.
34. X. C. Tai, O. W. Johansen, H. K. Dahle, and M. S. Espedal, *A characteristic domain splitting method for time-dependent convection diffusion problems*, Proceedings Eight International Conference on Domain Decomposition Methods, Beijing, 1995 (London) (R. Glowinski, J. Periaux, Z-C. Shi, and O. Widlund, eds.), J.Wiley, 1997.
35. T.Bu and L.B. Håøy, *On the importance of correct inclusion of capillary pressure in reservoir simulation*, Proceedings European IOR - Symposium, 1995.
36. C. J. van Duijn, J. Molenaar, and M. J. de Neef, *The effect of the capillary forces on immiscible two-phase flow in heterogenous porous media*, Transport in Porous Media **21** (1995), 71–93.

Department of Mathematics, University of Bergen, N-5008 Bergen, Norway
E-mail address: Magne.Espedal@mi.uib.no

Department of Mathematics, University of Bergen, N-5008 Bergen, Norway
E-mail address: Karl.Hersvik@mi.uib.no

Statoil a.s., N-5020 Bergen, Norway
E-mail address: BGE@statoil.no

License or copyright restrictions may apply to redistribution; see http://www.ams.org/publications/ebooks/terms